CrossMark

ORIGINAL PAPER

Mining-Induced Coal Permeability Change Under Different Mining Layouts

Zetian Zhang[1] · Ru Zhang[1] · Heping Xie[1] · Mingzhong Gao[1] · Jing Xie[1]

© Springer-Verlag Wien 2016

Abstract To comprehensively understand the mining-induced coal permeability change, a series of laboratory unloading experiments are conducted based on a simplifying assumption of the actual mining-induced stress evolution processes of three typical longwall mining layouts in China, i.e., non-pillar mining (NM), top-coal caving mining (TCM) and protective coal-seam mining (PCM). A theoretical expression of the mining-induced permeability change ratio (MPCR) is derived and validated by laboratory experiments and in situ observations. The mining-induced coal permeability variation under the three typical mining layouts is quantitatively analyzed using the MPCR based on the test results. The experimental results show that the mining-induced stress evolution processes of different mining layouts do have an influence on the mechanical behavior and evolution of MPCR of coal. The coal mass in the PCM simulation has the lowest stress concentration but the highest peak MPCR (approximately 4000 %), whereas the opposite trends are observed for the coal mass under NM. The results of the coal mass under TCM fall between those for PCM and NM. The evolution of the MPCR of coal under different layouts can be divided into three sections, i.e., stable increasing section, accelerated increasing section and reducing section, but the evolution processes are slightly different for the different mining layouts. A coal bed gas intensive extraction region is recommended based on the MPCR distribution of coal seams obtained by simplifying assumptions and the laboratory testing results. The presented results are also compared with existing conventional triaxial compression test results to fully comprehend the effect of actual mining-induced stress evolution on coal property tests.

Abbreviations

CBM	Coal bed methane
CTC	Conventional triaxial compression
MPCR	Mining-induced permeability change ratio
NM	Non-pillar mining
PCM	Protective coal-seam mining
TCM	Top-coal caving mining

1 Introduction

With the decreasing surface coal reserves and increasing energy demand caused by economic development, the mining depths and mining output of coal resources have been continuously increasing and are accompanied by an increasing number of disasters. Coal bed gas, which is mainly methane, has been one of the major hazards affecting safety and productivity in underground coal mines over the last century (Flores 1998). Meanwhile, coal bed methane (CBM) is also widely utilized as an unconventional natural gas, and it plays an important role in the energy supply and energy reserves in the USA, Australia, China and many other countries (Flores 1998; Moore 2012). Therefore, CBM extraction has been the subject of increasing attention around the world in recent decades.

✉ Ru Zhang
zhangru@scu.edu.cn

[1] State Key Laboratory of Hydraulics and Mountain River Engineering, College of Water Resource and Hydropower, Sichuan University, Chengdu 610065, China

🖄 Springer

One of the fundamental factors affecting the safety and efficiency of CBM extraction and underground coal mining is the permeability of coal mass. This property is an important parameter in evaluating the flow capacity of coal seams and is crucial for understanding CBM production (Palmer 2009; Ried et al. 1992; Sparks et al. 1995). The permeability evolution law greatly influences the strength and stability of coal seams (Wang et al. 2013c), the failure processes of coal masses, the occurrence of calamitous accidents and possible fault reactivation induced by deep underground CO_2 injection (Beamish and Crosdale 1998; Cappa and Rutqvist 2011).

Previous studies have shown that coal mass permeability is associated with many factors, such as the effective stress (Durucan and Edwards 1986), temperature condition (Perera et al. 2012), coal type, gas type (Robertson and Christiansen 2007), water content, fracture geometry (Wang et al. 2011), and CBM adsorption effect (Perera et al. 2011; Zhang et al. 2008; Zhu et al. 2013). The measurements of coal permeability in the laboratory show that the permeability of coal to adsorbing gases (e.g., CH_4 and CO_2) is time-dependent and lower than that of non-adsorbing or lightly adsorbing gases (e.g., nitrogen and argon) due to the swelling of the coal matrix (Chen et al. 2011; Siriwardane et al. 2009). Under constant temperature, the variation in confining stress has a significant influence on coal permeability (Dabbous et al. 1974; Somerton et al. 1975), which decreases with increasing pore pressure due to coal swelling (Mazumder and Wolf 2008; Pan et al. 2010; Wang et al. 2010, 2011). According to the experimental results based on laboratory or field observations, various stress-dependent coal permeability models have been proposed to analyze or forecast the deformation and permeability evolution of coal based on the idealized coal structure and specific conditions assumed (Chen et al. 2012; Cui and Bustin 2005; Gilman and Beckie 2000; Gray 1987; Harpalani and Chen 1997; Liu et al. 2010; Shi and Durucan 2004; Somerton et al. 1975). These studies have demonstrated that coal permeability is strongly stress-dependent. Therefore, analyses of the permeability evolution of coal seams should consider the mining-induced stress evolution process, because, the stress condition controls the stress-induced fracture geometry of the coal mass, which directly influences the transport properties of the coal seams (Gale 1982; Guo et al. 2012; Raven and Gale 1985; Somerton et al. 1975; Wang et al. 2013c).

The longwall mining method has been widely used in underground coal mines in the USA, Australia, China and many other countries. In the single coal seam longwall mining practice, the stress field near the mining surface is redistributed with increasing vertical stress acting upon the concerned near-face coal mass due to mining face advancement; meanwhile, the horizontal stress decreases relative to the initial stress condition (Li et al. 2015; Rezaei et al. 2015; Wang et al. 2013b; Xie et al. 2012; Yang et al. 2014). Concerning multi-coal seams, mining one coal seam introduces strata movement, stress redistribution and damage to adjacent coal seams (Guo et al. 2012; Suchowerska et al. 2013; Yang et al. 2011). Considering various geological conditions, different mining layouts have been used in mining practices to ensure safe and efficient excavation. Xie et al. summarized the properties of abutment pressure at a longwall coal face under three typical mining layouts, i.e., top-coal caving mining (TCM), non-pillar mining (NM) and protective coal-seam mining (PCM), and suggested a mining-induced stress state of the coal mass in front of the mining face to determine the loading and unloading parameters for a laboratory study subjected to different mining layouts (Xie et al. 2011, 2012).

TCM is usually used for thick coal seams to achieve high-yield, high-efficiency mining (Alehossein and Poulsen 2010; Whittaker 1974; Xie et al. 2009; Yasitli and Unver 2005). This layout typically positions a mining face at the bottom of the thick coal seam and caves the top coal mass, which is crushed by the mining area pressure or loose blasting, from the rear or top windows of the support frames. In NM, the coal mass near the mining face supports the superimposed abutment pressure from both the strike and dip directions of the coal seam, because the adjacent coal mass is mined without leaving coal pillars (Deng et al. 2003; Zhou et al. 2007). Therefore, the stress concentration factor of NM is higher than that of TCM. Knowing from the above two mining layouts, PCM is often used for multi-coal seams mining. In this layout, one coal seam (the protective coal seam) without risk of gas outburst is first mined, which relieves pressure and generates fractures in the coal seams above or below. As a result, when the protected coal seam is excavated, the stress concentration factor and gas outburst danger are considerably lower than in the case of directly mining the protected coal seam without mining the protective coal seam. According to existing research results (Chen et al. 2014; Kong et al. 2014; Yang et al. 2011), the technique of mining the protective seam, which is an efficient and fundamental precautionary measure, can significantly reduce the coal and gas outburst hazard and increase the permeability of protected coal seams. Accordingly, different mining layouts will induce different stress redistributions, stress concentration ranges and stress concentration coefficients near mining faces. The stress concentration coefficient K, an important parameter reflecting the influence of mining layouts on stress redistribution, defined as the ratio between the mining-induced peak stress and the pre-mining in situ stress, ranges from 1.5 to 6 (Ouyang et al. 2009; Singh

et al. 2011; Yang et al. 2011). Previous studies have shown that the mining-induced peak stress is approximately 2.2–3.5, 1.7–2.7 and 1.4–2.4 times the initial confining stress under NM, TCM and PCM, respectively (Xie et al. 2012, 2011; Yang et al. 2011). Studies on the stress redistribution and gas flow of coal seams under different mining layouts are mainly conducted by numerical simulation or field observation (Adhikary and Guo 2015). Nevertheless, to better understand the mechanism of pressure relief and permeability enhancement, experimental laboratory analyses are crucial for testing and verifying the results obtained by the abovementioned means.

Coal mass permeability is a function of the fracture system determined by the fracture geometry (Wang et al. 2011; Zhang et al. 2015b), which is strongly influenced by the stress evolution process. The coal mass is damaged by the mining-induced stress, and the fracture geometry and coal mass permeability change, because, the mining-induced fractures and pores are connected to form effective flow paths or compressed to closure (Wang et al. 2013a; Zhang et al. 2015a). However, the majority of the existing studies concerning the permeability evolution of coal masses have been conducted by conventional triaxial compression (CTC) tests (Cai et al. 2014; Meng and Li 2013; Wang et al. 2011, 2013c), neglecting the distinction between actual mining-induced stress evolution and the conventional triaxial compression test loading process, which leads to significantly different experimental results (Wang et al. 2013c; Xie et al. 2011, 2012). The CTC test results can only reflect the transport property of coal as a type of rock-like material. Additionally, coal mass permeability is often treated as a constant in the design of mining practices, which ignores the mining-induced permeability change, and the theoretical studies conducted to date are insufficient for quantitatively describing the mining-induced amount. Xie et al. first noted that the variation of mining-induced permeability can be quantitatively defined as the mining-induced permeability change ratio (MPCR) ω, which represents the change in permeability per unit of volumetric change in coal (Xie et al. 2013). Additionally, Xie et al. designated a new definition of the MPCR as a relative increment of coal permeability in a representative volumetric element induced by mining, considering the fracture bodies as the main galleries for gas migration (Xie et al. 2015). According to these studies, the MPCR ω can be plausibly and practically determined by laboratory and field tests. It can also represent the quantitative influence on the coal permeability caused by the evolution of the mining-induced fractures, and provide strong scientific support for the quantitative evaluation of the effect on the coal permeability and the CBM extraction arrangement.

Accordingly, more attention should be paid to the influence of the mining-induced stress condition on the mechanical properties and variation in the permeation capacity of coal. Different mining layouts induce different stress conditions and damage processes in the coal; hence, this study focuses on the influence of mining layouts on the permeability variation of coal. The MPCR is used to quantitatively describe the effect of the mining layout on the evolution of mining-induced coal permeation capacity change. To better understand the evolution of the mining-induced coal permeability under different mining layouts, a series of laboratory experiments are conducted to simulate the simplified stress evolution processes of different mining layouts.

2 Theoretical Expression of MPCR Based on Darcy's Law

Assuming that the permeation of methane through a coal specimen is an isothermal process and that the ideal gas law is applicable, the equation for the horizontal linear steady permeation of compressive gas based on Darcy's law and Boyle's law, which can be used for permeation data processing, is as follows (Somerton et al. 1975):

$$k = \frac{2qpq_{air}\mu L}{A\left(p_1^2 - p_2^2\right)} \tag{1}$$

where k is the permeability of the sample (m^2), q is the flow rate (m^3/s), p_{air} is the atmospheric pressure (MPa), μ is the viscosity of the fluid (MPa·s), L is the length of the sample (m), A is the cross-sectional area of the sample (m^2), and p_1 and p_2 are the upstream and downstream pore pressures (MPa), respectively.

The initial permeability k_0 of the coal mass to gas is

$$k_0 = \frac{2q_0pq_{air}\mu_0 L_0}{A_0\left(p_1^2 - p_2^2\right)} \tag{2}$$

where the subscript 0 denotes the initial condition.

Permeability measurements in coal can be influenced by the Klinkenberg effect (Klinkenberg 1941; Liu et al. 2014; Somerton et al. 1975; Zhu et al. 2007). When the mean free path of the gas molecules is of the same order as the flow path dimension, the gas molecules have an appreciable interaction (i.e., collisions) with the flow path surfaces. The relationship between the effective permeability k_m in the case of slip and the absolute permeability k is given as follows:

$$k_m = k\left(1 + \frac{b}{p}\right) \tag{3}$$

where k is the absolute gas permeability (m^2) under a high gas pressure, where the Klinkenberg effect is negligible, and b is the Klinkenberg coefficient (Pa), which depends on the mean free path of the gas molecules. The mean free

path of the gas molecules depends on the pressure, temperature, and molecular weight of the gas. In this study, the Klinkenberg effect is subtracted from all permeability data using $b = 1.85 \times 10^5$ Pa.

In mining practices, k is typically treated as a constant, thus ignoring the effect of mining-induced stress change. Coal masses are known for their dual-porosity characteristics, and with the mining effect, their initial pores and fractures expand, connect. and ultimately generate a complex fracture network (Zhang et al. 2015a, b). The permeability of a coal mass is a function of its fracture system, which is seriously deformed and damaged by mining-induced stress. Therefore, k is related to the evolution of the mining-induced stress. However, few theories quantitatively describe the mining-induced variation in coal permeability. Xie et al. first proposed two different definitions for MPCR to quantitatively describe the change in coal permeability (Xie et al. 2013, 2015), which are stated in the introduction section. In a simultaneous exploitation of coal and gas, the variation of coal permeability is considerably important, and the gas flow in the severely damaged coal mass with complex fracture networks is macroscopically satisfied by Darcy's law. Therefore, based on this mathematical description, the MPCR ω can be defined as follows (Xie et al. 2015):

$$\omega = \frac{k_m - k_{m0}}{k_{m0}} = \frac{k}{k_0} - 1 \tag{4}$$

where ω is a dimensionless quantity expressed as a percentage.

The difference in the gas flow pressure is fixed, and the viscosity of gas is constant throughout the tests. Inserting Eqs. 1 and 2 into Eq. 4 yields

$$\omega = \frac{q(1-\varepsilon_x)^2}{q_0(1-\varepsilon_v)} - 1 \tag{5}$$

where $\varepsilon_v = -(V - V_0)/V_0$ is the volumetric strain of coal mass and $\varepsilon_x = -(L - L_0)/L_0$ is the strain of the coal specimen in the direction of gas flow, which is also the axial direction in this study. Equation 5 can be used for analyzing the testing results of any specific loading scenario.

Considering the hydrostatic stress condition of the coal mass in an underground deep mine, the volumetric strain ε_v is three times the axial strain of the coal specimen ε_x. Then ω can be written as

$$\omega = \frac{q(3-\varepsilon_x)^2}{9q_0(1-\varepsilon_v)} - 1 \tag{6}$$

From Eqs. 5 and 6, the mining-induced coal permeability has a simple form and a relationship with the gas

flow rate and strain. There properties can be more easily measured in situ than the permeability and can be used to estimate the permeability variation of the coal seams. In PCM simulation, the pre-mining unloading expansion deformation has been added as the initial deformation amount of the coal mining simulation stage to consider the effect of mining the protective coal seam.

3 Experimental Techniques

3.1 Specimen Property and Preparation

The coal samples are anthracite blocks collected from the #4 coal seam of the Baijiao mine in Yibin, China, according to the description of Chinese national standard GB/T 23561.1-2009. Table 1 summarizes the properties and test information of the coal specimens, and the pure gas used in this study is CH_4 at purities of 99.99 %. The coal specimens were drilled from the coal samples as cylinders with dimensions of $\Phi 50$ mm $\times H100$ mm according to the description of ASTM standard D4543-08. The average uniaxial compressive strength of the coal specimens is 10.1 MPa at an axial strain rate of 10^{-4}, and the average triaxial compressive strength is 96.6 MPa using the same loading rate with a confining stress of 25 MPa.

Table 1 Properties of the Baijiao anthracite samples

| Fixed carbon	Volatile matter	Ash		
Proximate analysis				
75.17 %	7.64 %	16.38 %		
Carbon	Hydrogen	Nitrogen	Sulfur	Oxygen
Ultimate analysis (Cao et al. 2000)				
89.56 %	2.7 %	1.13 %	2.97 %	3.64 %
Kaolinite	Quartz	Calcite	Others	
Constituent of mineral matter				
5.58 %	11.74 %	5.04 %	77.64 %	
Sample no.	Diameter (mm)	Length (mm)	Density (kg/m³)	
Sample physical properties				
N-2-1	50.14	97.23	1435.2	
T-2-1	50.09	99.42	1498.8	
T-2-2	50.16	98.23	1479.6	
P-2-1	50.17	99.97	1454.1	
P-2-2	50.07	100.09	1478.0	
P-2-3	50.09	99.86	1458.8	
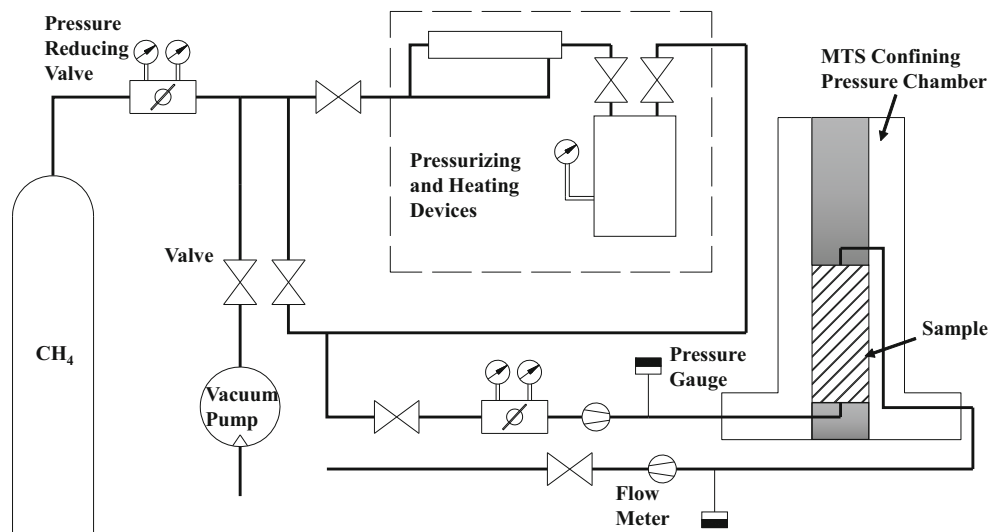
Fig. 1 Schematic diagram of the external gas flow system (Zhang et al. 2014b)

3.2 Apparatus

A redesigned MTS815 rock mechanics testing system (Sichuan University, Chengdu, China) equipped with a self-designed external gas flow system was employed to conduct the experiments (Zhang et al. 2014b). This system has a high stiffness (10.5×10^9 N/m), high load-sensing accuracy (10 N) and high deformation-sensing accuracy (1 μm). The maximum axial compression load of the testing system is 4600 kN. The testing ranges of the confining stress and the axial and circumferential deformation extensometer are 0–140 MPa, −2.5 to +5.0 mm and −2.5 to +8.0 mm, respectively. The self-designed gas flow system is schematically shown in Fig. 1. The testing range for the pore pressure is 0.3–20 MPa, and the gas can be heated from room temperature to 70 °C. The testing range of the methane flow rate is 5–5000 mL/min with a high sensing accuracy of 1 ‰ full scale.

3.3 Experimental Procedure

3.3.1 Simplifying Assumptions of the Longwall Mining-Induced Stress Evolution Process

Due to coal seam excavation or mining face advancement, the stress field near the mining face is redistributed (Wang et al. 2013b). Based on Xie's study, assuming that the deep coal seam originates in a hydrostatic pressure state, the distribution of pressure ahead of the mining face (Fig. 2) can be simplified as follows: with decreasing distance from the mining face, the vertical stress acting on the coal seam gradually increases to a peak stress from the hydrostatic pressure state and then quickly decreases due to coal-mass damage; the horizontal stress gradually decreases to 0 from
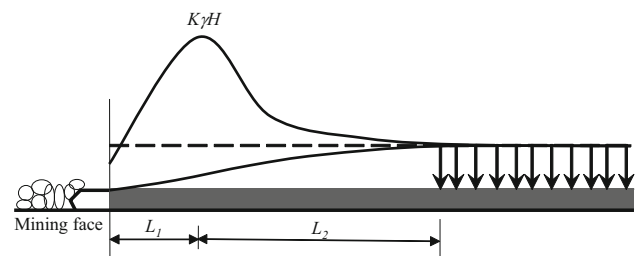

Fig. 2 Distribution of abutment pressure ahead of the mining face (Xie et al. 2011)

the hydrostatic pressure state (pressure relief), ignoring the stress rotation and fluctuation near the mining face due to coal and rock failure (Diederichs et al. 2004). The majority of the excavated coal mass of longwall mining has experienced such a stress evolution process. This process is schematically shown in Fig. 2, where γ is the average unit of overburden weight, H is the mining depth, K is the abutment pressure coefficient, and L_1 and L_2 are the lengths of the abutment pressure of the decreasing and increasing sections, respectively.

3.3.2 Experimental Simulation Method of Different Mining Layouts

To simulate different mining layouts in the laboratory, Xie et al. have suggested the loading paths (Fig. 3) according to the simplifying assumption of the longwall mining-induced stress evolution process acting upon the coal mass, as discussed above. The loading paths and rates of the corresponding mining layouts, i.e., TCM, NM and PCM, are shown in Fig. 3 and Table 2. In this study, the specific loading paths are the same as in Xie's work, in which the
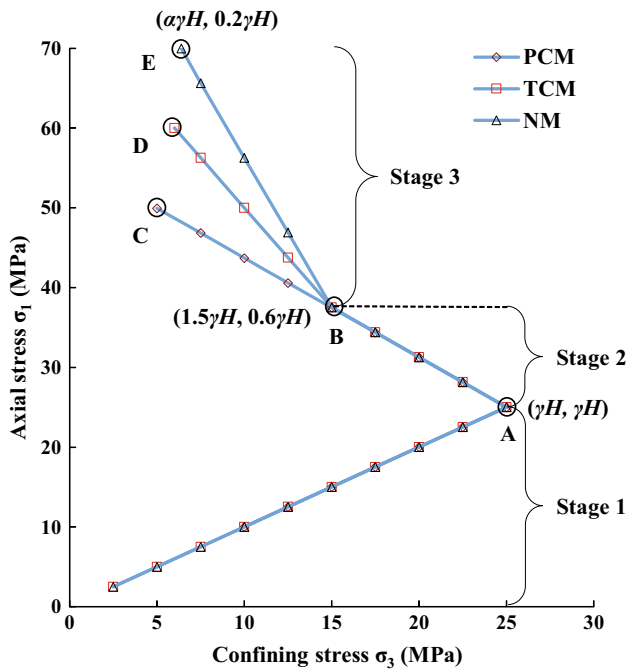
Fig. 3 Loading schemes of the different mining layouts (Xie et al. 2012)

loading paths are divided into three stages to simulate the mining-induced stress evolution process (Xie et al. 2011, 2012). The detailed setup can be briefly stated as follows:

Stage 1 Assume that the coal mass is initially in a hydrostatic stress status and the depth of the coal seams is 1000 m with a vertical stress gradient of 25 kPa/m. The confining stress is loaded at the same rate of 3 MPa/min to point A ($\sigma_1 = \sigma_3 = 25$ MPa) in Fig. 3.

Stage 2 To simulate the forepart confining stress unloading and axial stress increasing process (line segment AB in Fig. 3), the axial stress is loaded to 37.5 MPa at a

deviatoric stress loading rate of 2.25 MPa/min, meanwhile, the confining stress is unloaded to 15 MPa with a rate of 1 MPa/min. The stress environment of the coal sample gradually changes from a hydrostatic condition to a stress status with a stress concentration coefficient K equal to 1.5.

Stage 3 To simulate the different stress concentrations and failure processes of coal mass induced by different mining layouts, the deviatoric stress loading rate is set to 2.25 MPa/min in PCM, 3.5 MPa/min in TCM and 4.75 MPa/min in NM. The confining stress unloading rate is held at 1 MPa/min.

We make two modifications of his work. We conducted the experiments with a fixed gas flow pressure difference of 2 MPa to show the permeability evolution and gas-influenced properties of the coal mass under different mining layouts. We also added a pre-mining unloading-expansion process simulation of the protected coal seam to comprehensively understand the mining-induced permeability in protected gassy coal seams.

3.3.3 Experimental Simulation Method of the Pre-Mining Unloading-Expansion Process in PCM

To simulate the pre-mining unloading-expansion process of the protected coal seam, we consider the results given by the existing numerical simulation, the model experiment, and site observation, due to the mining of the protective coal seam (Chen et al. 2014; Guo et al. 2012; Liu et al. 2011; Wang et al. 2008; Yang et al. 2011; Zhang et al. 2014a). Here, the pressure relief and permeability improvement effect is one of the key issues in the protective seam mining (Chen et al. 2013), and the pre-mining protected coal seam in PCM typically has four deformation sections: compression expansion, unloading expansion deformation increasing, expansion deformation decreasing, and expansion deformation stabilizing. As a result, the

Table 2 Testing parameters and main results

Simulated mining layout	Test number	Stage[c]1 confining stress loading rate (MPa/min)	Stage 2 and 3 confining stress unloading rate (MPa/min)	Stage 2 deviatoric stress loading rate (MPa/min)	Stage 3 deviatoric stress loading rate (MPa/min)	Peak stress (MPa)	Confining stress at peak stress (MPa)	Axial strain at peak stress (%)	Initial permeability (m²)	Peak MPCR (%)
NM	N-2-1	3.0	1.0	2.25	4.75	58.67	9.67	0.858	5.89E−17	304
TCM	T-2-1[a]	3.0	1.0	2.25	3.50	50.77	9.84	0.646	4.49E−17	–
	T-2-2	3.0	1.0	2.25	3.50	58.04	7.18	0.713	6.32E−17	590
PCM	P-2-1[b]	3.0	1.0	2.25	2.25	46.35	8.88	0.429	2.60E−17	1669
	P-2-2	3.0	1.0	2.25	2.25	44.28	10.20	0.652	3.87E−17	4138
	P-2-3	3.0	1.0	2.25	2.25	49.40	6.33	0.901	5.43E−17	3764

[a] The permeation data of specimen T-2-1 was not recorded due to equipment failure

[b] The specimen P-2-1 is simulated without a pre-mining unloading-expansion process as a comparison

[c] The test stages are shown in Fig. 3

laboratory simulation of the pre-mining protected coal seam deformation behavior includes at least three sections: vertical compression, unloading-expansion and recompression to a stable state. The simulation procedure of the pre-mining unloading-expansion process for the protected coal seam can then be established as follows:

1. Confining stress loading stage (Recover the initial stress state of the coal mass)

   Assume that the depth of the coal seams is 1000 m with a vertical stress gradient of 25 kPa/m and that the coal mass is in a hydrostatic stress state. With a loading rate of 3 MPa/min, the confining stress is increased to 25 MPa and is shown as line segment OA' in Fig. 4.

2. Vertical loading stage (Simulate the compression expansion section)

   Simulate the expansion induced by axial compression under the protected coal seam mining, in which the confining stress is held constant and the axial stress increases. The confining stress is held constant, and the axial stress σ_1 is increased to 37.5 MPa (A'B' in Fig. 4) with a loading rate of 3 MPa/min.

3. Circumferential unloading stage (Simulate the unloading expansion deformation increasing section)

   Simulate the expansion induced by circumferential pressure relief, in which the deviatoric stress ($\sigma_1-\sigma_3$) is held constant and the confining stress is decreased until the coal samples reach the yield deformation section with an unloading speed of 1 MPa/min (B'C' in Fig. 4).

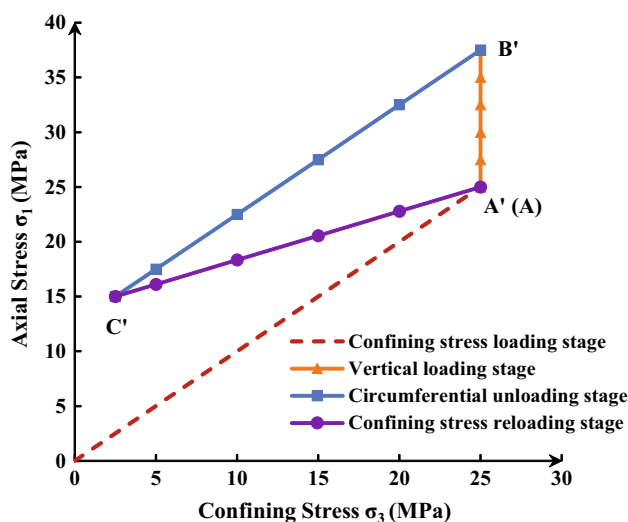4. Confining stress reloading stage (Simulate the expansion deformation decreasing section)

Fig. 4 Simulation procedure of the pre-mining unloading-expansion process for the protected coal seam

Simulate the expansion-deformation stabilizing process by reloading the confining stress, increasing the confining stress σ_3 to 25 MPa with a reloading rate of 3 MPa/min. The ($\sigma_1-\sigma_3$) decreases to 0 MPa (C'A in Fig. 4), assuming that the final stress condition returns to the initial hydrostatic condition. Next, the axial and circumferential extensometers are reset, and the excavation of the protected coal seam itself is simulated with the loading path A–B–C shown in Fig. 3.

During the experiments simulating the different mining layouts with a fixed flow gas pressure difference, the vertical loading stage of PCM, and stage 2 of NM and TCM begin after the saturation adsorption of coal is accomplished. Devices with high permeability and pressure sensing accuracy (1 ‰) are employed to record the testing data of the external gas flow system. The deformation data are recorded by extensometers of the MTS815 rock mechanics testing system. The evolution of the MPCR and mechanical behavior of coal mass can be obtained from the testing results.

4 Results and Analyses

4.1 Effect of Mining Layouts on the Mechanical Behavior of Coal Mass

The basic information, loading conditions and main results of the tested coal samples are summarized in Tables 1 and 2. The gas pressure difference and confining stress unloading rate are held constant throughout the test at 2 MPa and 1 MPa/min, respectively, and the deviatoric stress loading rates in stages 2 and 3 (Fig. 3) are established according to the experimental procedures. Figure 5 shows the changing rule of the mechanical parameters of the coal samples under the different mining layouts.

First, the effect of mining layouts on the strength of coal masses can be explored in Fig. 5a. The average peak stress of the coal specimens under PCM, TCM, and NM is 46.68, 54.41, and 58.67 MPa, respectively, which indicates that the corresponding stress concentration factors (K) at peak stress under each mining layout are 1.87, 2.18 and 2.35, respectively. These values are consistent with the testing range of the stress concentration coefficient determined by previous researchers under the corresponding mining layouts. Due to the superimposed abutment pressure, the coal seam of NM has the highest stress concentration factor, whereas the coal seam of PCM has the lowest stress concentration factor because of the pre-mining stress release. The peak stress and corresponding stress concentration factor under the different mining layouts are less than those found in experiments conducted without gas pressure using
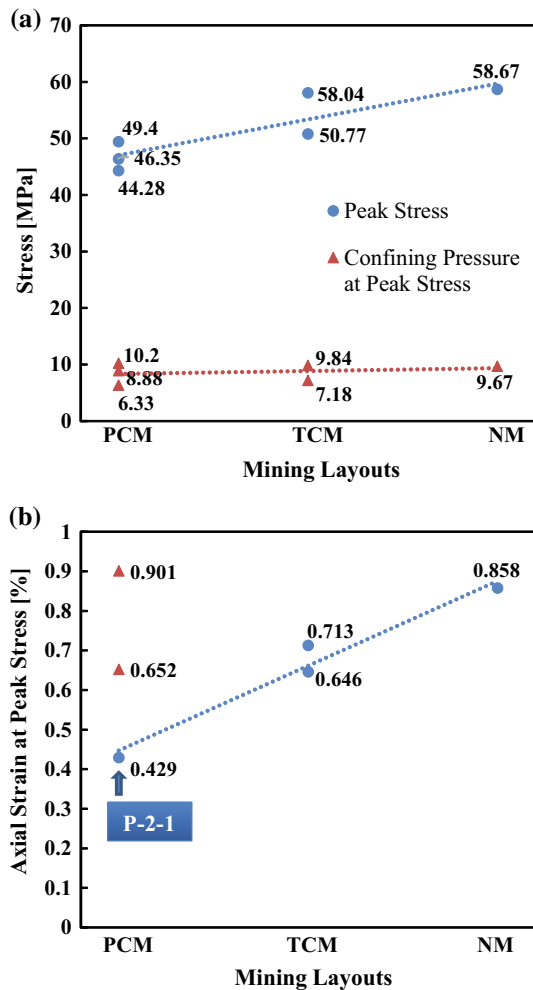
Fig. 5 Mechanical parameters of coal specimens under the different mining layouts: **a** peak stress and corresponding confining stress; **b** axial strain at the peak stress

simulated without a pre-mining unloading-expansion process, differ only slightly from the values for the two other specimens used in the simulations. This result indicates that the simulation of the pre-mining unloading-expansion process of PCM does not notably impact the strength of coal in the simulation of coal seams excavated under the different mining layouts. The coal mass of the protected coal seam undergoing the pre-mining unloading-expansion process does not decrease in strength before excavation.

Second, the effect of the mining layouts on the axial deformation characteristics of the coal mass can be determined according to Fig. 5b. The average axial strains of the coal specimens under PCM (without simulating the evolution of pre-mining stress), TCM, and NM are approximately 0.43, 0.68 and 0.86 %, respectively, and increase in the order of PCM, TCM, and NM (increasing deviatoric stress loading rate). Specimens P-2-2 and P-2-3 (simulating the evolution of pre-mining stress) have a larger axial strain than P-2-1. Considering the strength testing results, the scheduled simulation of the pre-mining unloading-expansion process enhances the deformability of the coal mass while only slightly influencing the strength. In other words, mining the protective coal seam can enhance the deformability of the coal mass in protected coal seams without greatly influencing the strength.

4.2 MPCR Evolution of Coal Mass and Validation

The mining-induced coal permeability under the different mining layouts can be analyzed according to Fig. 6. Table 2 shows that the average initial permeability of the coal specimens is approximately 4.77×10^{-17} m^2. The MPCR of coal specimens is calculated using Eq. 5. Among the samples, the peak MPCR is lowest for sample N-2-1 (304 %) and highest for sample P-2-2 (4138 %). The peak

Tashan coal (Xie et al. 2011, 2012), which may result from the coal type but more likely results from the decrease in effective confining stress due to the application of gas pressure. As shown in Fig. 5a, the confining stress corresponding to the peak stress under the different mining layouts does not increase in the order of PCM, TCM, and NM (increasing deviatoric stress loading rate) but rather stays in the range of 6.33–10.20 MPa, which is higher than in the experiments conducted under no gas pressure using Tashan coal (Xie et al. 2011, 2012). This observation indicates that compared with a low-gas coal seam, a gassy coal seam is likely to be more severely damaged under a relatively high confining stress. Additionally, the existence of gas in coal seams can decrease the peak stress of the coal mass and increase the risk of coal damage under the high confining stress, potentially resulting in mining disasters. Figure 5a illustrates that the peak strength and corresponding confining stress of specimen P-2-1, which is
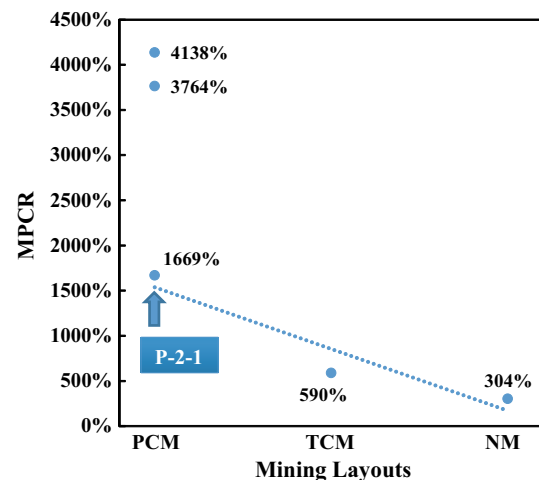

Fig. 6 Peak MPCR of the coal specimen under the different mining layouts

MPCR of sample P-2-1, which is simulated without a pre-mining unloading-expansion process for comparison, is 1669 %, corresponding to approximately 40.3 % and 44.3 % of the values for samples P-2-2 and P-2-3, respectively. Accordingly, the scheduled simulation of the pre-mining unloading-expansion process induces irreversible deformation and pre-mining damage to the coal mass, which enhances the deformability of the coal mass and the range of permeability variation. Mining the protective coal seam can induce pre-mining damage in protected coal seams and increase their deformability and permeability.

As per the experimental procedure for the different mining layouts, the coal specimens experience a complete mining-induced stress evolution process, and the complete evolution processes of the MPCR are recorded by the testing system. Figure 7 shows the MPCR evolution process of the coal mass under the different mining layouts and the relationships between axial stress and axial strain, and between volumetric strain and axial strain. The coal mass of the protected coal seam in the PCM simulation has a residual deformation after the simulation of pre-mining stress evolution, which has been substituted into Eq. 5 to evaluate the pre-mining enhanced permeability induced by the protective coal seam mining. For the typical sample P-2-3 in Fig. 7, the residual axial strain and volumetric strain are 0.186 and −0.104 %, respectively, resulting in a pre-mining relative increment of coal permeability ω of 200 %.

According to Fig. 7, the axial stress–strain curves of the coal mass under the different mining layouts can be clearly divided into three sections: elastic deformation, yield deformation and post-peak deformation. Compared with the axial strain, the volumetric strain ε_v and MPCR ω have similar evolution processes, which can also be divided into three sections, i.e., stable increasing, accelerated increasing and decreasing, but the evolution processes are slightly different for the different mining layouts.

First, according to Fig. 7a, the ε_v and ω of the coal mass under NM have a linear growth trend with the increase in axial strain in the stable increasing section. ε_v and ω increase gradually from 0 to −0.428 % and 52.2 %, respectively, upon an axial strain increment of 0.5 %. In the stable increasing section, the initial pores and fractures in the coal mass steadily deform and extend with increasing axial stress. The permeability of the coal mass monotonically increases throughout the loading due to a strong confining-unloading-expansion effect. Then, the growth of ε_v occurs at a higher and steadily increasing rate, whereas the growth rate of ω increases before reaching the peak stress in the accelerated increasing section. Meanwhile, the corresponding stress–strain curve is in the yield deformation section. In this section, the pores and fractures in the coal mass exhibit accelerated development and propagation, and the number of effective flow paths also rapidly increases. The peak coal mass permeability appears before reaching the peak stress, and the corresponding ω is 304 %. Finally, in the post-peak deformation section, the coal mass is damaged, and its permeability gradually decreases to approximately 3.5 times its initial amount.

Second, according to Fig. 7b, the ε_v and ω of the coal mass under TCM increase linearly with the increase in
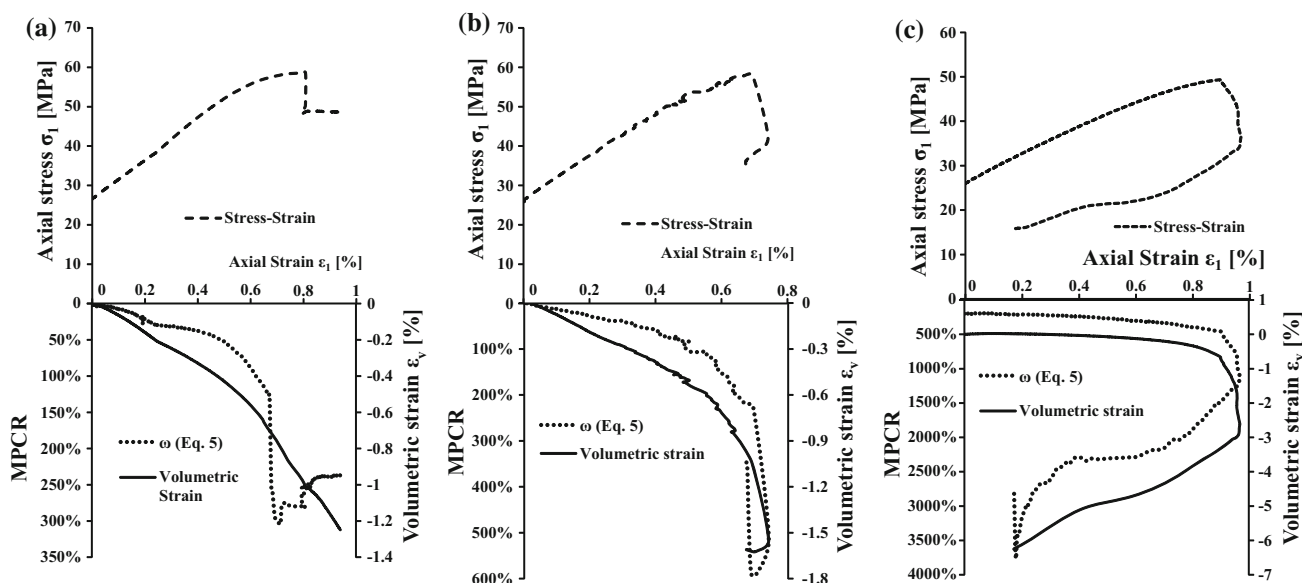

Fig. 7 Coal mass MPCR with axial and volumetric strain under the different mining layouts: a N-2-1 under NM, b T-2-2 under TCM, c P-2-3 under PCM

axial strain in the stable increasing section. ε_v and ω increase gradually from 0 to -0.535 % and 104 %, respectively, with an axial strain increment of 0.5 %. In the stable increasing section, the ε_v and ω of the coal mass have a higher increasing rate in the TCM simulation than in the NM simulation because, the TCM conditions include less axial compression with the same confining stress unloading effect but lower axial stress concentration. The coal mass permeability also increases continuously throughout the loading process due to a strong confining-unloading-expansion effect. Then, the growth rates of ε_v and ω increase before reaching the peak stress in the accelerated increasing section, whereas the corresponding stress–strain curve is in the yield deformation section. After the peak stress is reached, the coal mass expands rapidly in the circumferential direction, and ε_v increases by -2.3 % with an axial strain increment of 0.05 %; meanwhile, ω increases considerably from 228 to 590 %. Afterward, ε_v remains unchanged at approximately 1.6 %, and ω decreases until the coal mass is fully crushed and the effective flow paths vanish.

Third, the deformation and permeation properties of the coal mass under PCM can be obtained from Fig. 7c. Due to the residual deformation after the simulation of pre-mining stress evolution, the ω of the coal mass under PCM increases by 200 %, which has been added as an initial relative increment in the coal mass permeability. The ε_v and ω of the coal mass under PCM exhibit a steady linear growth with increasing axial strain in the stable increasing section. ε_v and ω increase from -0.104 and 200 % to -0.732 and 452 %, respectively, in a stable manner upon an axial strain increment of 0.9 %. Accordingly, the coal mass under PCM has the smallest change in volumetric strain and the highest increase in ω per unit of axial strain increment, which contributes to the pre-mining unloading-expansion induced by the protective coal seam mining and the lowest axial stress concentration of the protected coal seam excavation. The growth rates of ε_v and ω then increase after reaching the peak stress in the accelerated increasing section, whereas the corresponding stress–strain curve is in the post-peak deformation section. The coal mass is gradually damaged by the axial compression and hoop unloading, with an enormous increase in ω from 452 to 3764 % in the accelerated increasing section, and then, a decrease in ω to approximately 2800 % as the coal mass is crushed in the decreasing section. Accordingly, the distance between the peak stress and the inflection point of the coal mass, where the rates of increase in ε_v and ω begin an accelerated increase, successively increases in the order of NM, TCM and PCM, and the PCM is the mining layout with the greatest increase in coal mass permeability.

Additionally, the gas flow rate evolution process of the coal mass during the mining simulation can be regarded as
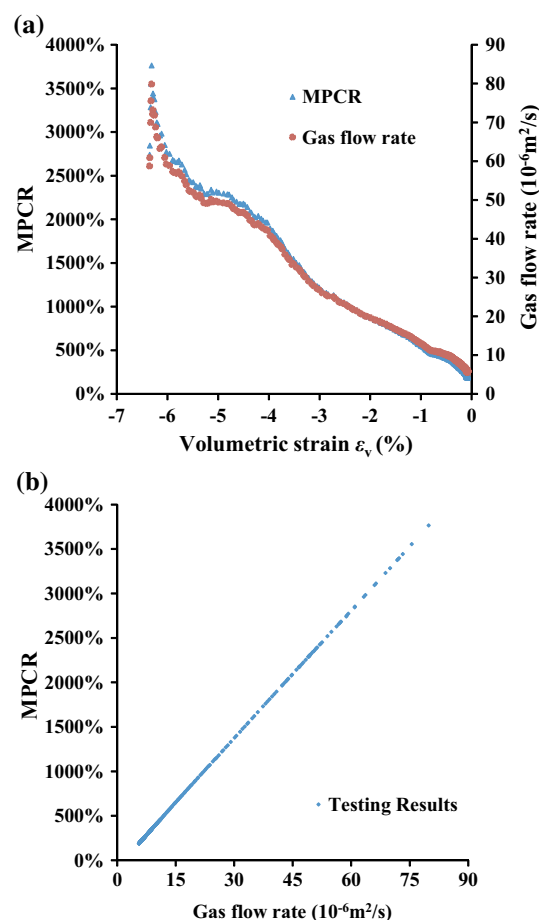

Fig. 8 Results of typical specimen P-2-3 for the validation of MPCR: **a** evolution process of MPCR and gas flow rate with volumetric strain; **b** relationship between MPCR and gas flow rate

a verification index for validating the plausibility of the proposed theoretical expression of MPCR based on Darcy's law, which is used to quantitatively describe the change in the coal permeability. Figure 8 shows that the MPCR correlates well with the gas flow rate (accuracy of 10^{-6} m^3/s), with the two factors exhibiting a linear relationship. Specifically, a higher MPCR leads to a higher gas flow rate from the testing results. Therefore, the MPCR can be used to quantitatively describe the permeability increment, and laboratory tests verify that a theory based on this new mechanical quantity is plausible.

4.3 MPCR of Coal Seams Under Different Mining Layouts and Engineering Applications

Assuming that the distance from the coal mass to the mining face corresponds with the loading time in the simulations of the different mining layouts, which are established according to the simplifying assumption of the mining-induced stress environment of the in situ coal mass, the laboratory testing results can be applied to the field coal
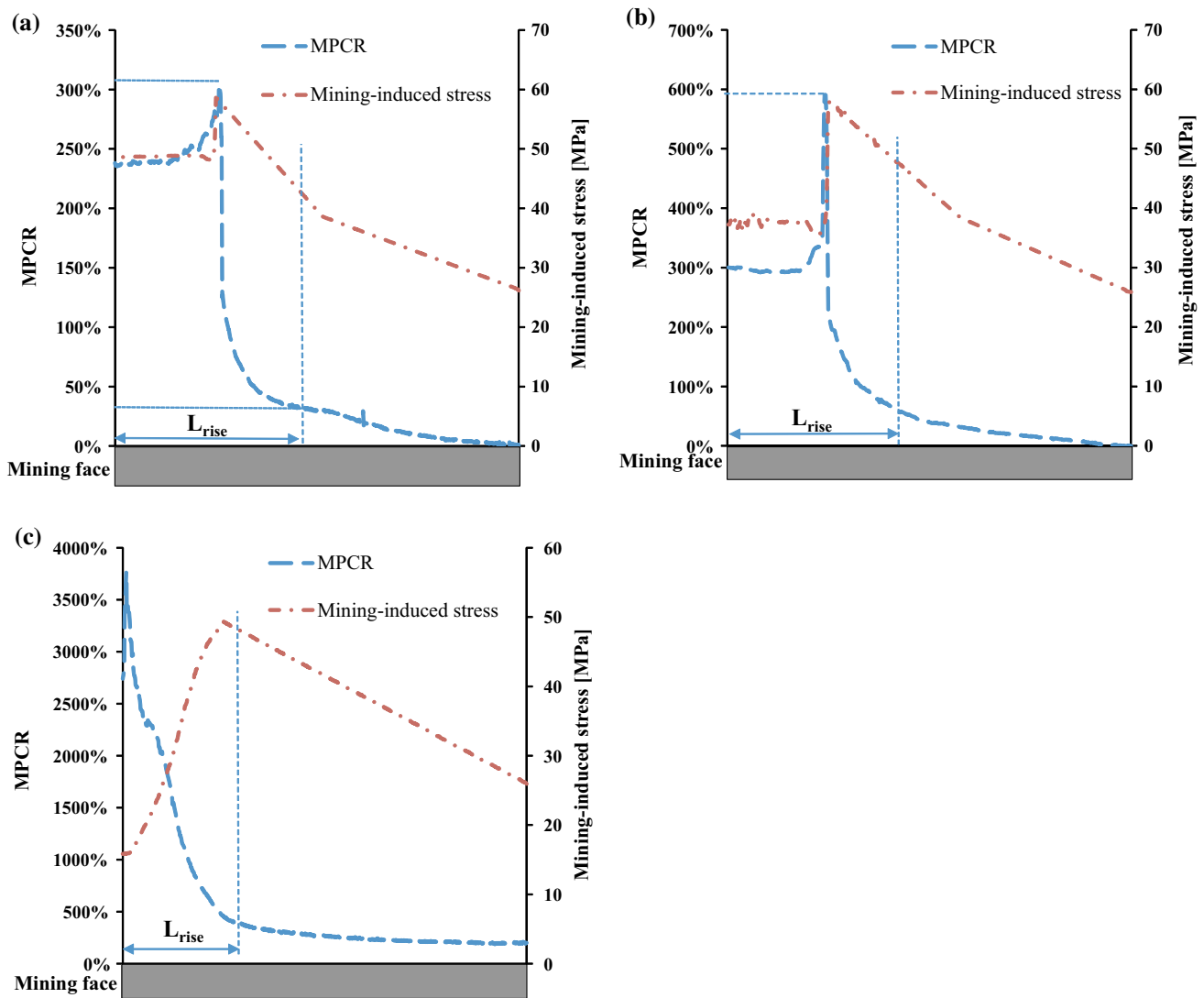
Fig. 9 Mining-induced stress and MPCR of coal seams estimated by experimental results under different mining layouts versus the distance from the mining face: **a** N-2-1 under NM; **b** T-2-2 under TCM; **c** P-2-3 under PCM

seams for the mining-induced stress and MPCR distribution analyses. For a direct viewing comparison, assuming that the distances from the peak stress of the abutment pressure to the mining face under the different mining layouts are equal, the corresponding testing data have been divided into two sections, i.e., the post-peak section and the pre-peak section. The loading time linearly corresponds to the distance from the concerned coal mass to the mining face in the two sections, where the coal samples under a specific stress state in the tests represent coal mass at a certain distance from the mining face.

Figure 9 shows a schematic of the mining-induced stress and MPCR of the coal seam ω versus the distance from the mining face estimated from the experimental results for the different mining layouts. According to Fig. 9, the distribution of ω in the coal seams can be summarized by the same

three sections as the ω-ε_1 curve shown in Fig. 7, i.e., stable increasing section, accelerated increasing section, and decreasing section. In the stable increasing section, the MPCR of the coal seam increases linearly with decreasing distance from the mining face. Specifically, if the coal mass in this section is closer to the mining face, it will have a better permeation capacity due to the stable deformation and failure in the coal seam. In the accelerated increasing section, the MPCR of the coal seam increases exponentially with decreasing distance from the mining face. The coal mass in this section is seriously damaged by the mining-induced stress, and a vast number of effective flow paths are generated in the coal seam, resulting in a steep rise in MPCR. In the decreasing section, the MPCR of the coal seam decreases with the distance from the mining face as a result of severe coal mass damage and the decline in effective flow paths.

The distance between the inflection point, where the growth rates of ω accelerate, and the mining face is defined as L_{rise}. As shown in Fig. 9, L_{rise} decreases in the order of NM, TCM, and PCM, and the MPCR of the coal seam in the range of L_{rise} is larger than 30 %. Considering the test results and analyses above, the coal mass in the stress concentration region of the coal seams is seriously damaged, and a mass of effective CBM flow paths is generated. Therefore, the CBM extraction under NM and TCM should be strengthened in the range of L_{rise}. However, the coal mass permeability in the protected coal seams is significantly higher for the PCM than for the other two mining layouts. The initial MPCR of the protected coal seams is greater than 200 %. Meanwhile, the CBM extraction in the protected coal seams can be started immediately after the extraction section undergoes the pre-mining unloading-expansion process induced by the mining of the protective coal seam. Therefore, the ascertainment of L_{rise} is of great value for determining the time and emphasis range of the CBM extraction. The effect of the measures to enhance the permeability of the coal seams can be quantitatively described by the MPCR and the range of L_{rise}. For in situ observations, it is difficult to measure the permeability in coal seams but easy to test mining-induced stress; therefore, according to the correspondence between the mining-induced stress and MPCR of coal seams, the L_{rise} under specific mining layouts can be assessed using the corresponding in situ mining-induced stress testing data.

Overall, the MPCR can quantitatively describe the variation in the permeability of the coal seam, and ascertaining the L_{rise} is helpful and instructional for optimizing the CBM extraction in coal seams under the different mining layouts.

5 Discussion

5.1 Effect of Real Mining-Induced Stress

According to the testing results and analyses of the variation in MPCR of coal mass, we can directly determine how the MPCR results differ from the results of typical conventional triaxial compression (CTC) tests (Wang et al. 2013c). In CTC tests, the permeability of the coal mass typically decreases initially and then begins to increase after reaching the yield deformation stage. However, in this study, the permeability of the coal mass continuously increases before reaching the peak stress, and then, decreases in the post-peak section. Some previous studies on mining-induced stresses and permeability present a similar mining-induced stress and pore pressure evolution

process ahead of the mining face but with a permeability distribution completely different from the results in this study. Such differences may result from the initial experimental setup and an underestimation of the unloading effect. The coal mass permeability is strongly stress-dependent, and related studies should consider the influence of the actual mining-induced stress evolution process. In this study, the actual mining-induced stress environment of coal seams is sufficiently considered, and all the tests are conducted according to its simplifying assumption that the circumferential stress is continuously unloading and the abutment pressure (vertical stress) gradually increases to a peak stress from the hydrostatic pressure state before transforming into an unloading state due to coal-mass damage. In the CTC test, the circumferential stress is fixed and the coal mass is regarded as a rock-like material without considering the effect of actual mining-induced stress. Considering that the mechanical properties and coal mass permeability are strongly stress-dependent, the actual mining-induced stress environment has a predictably marked effect on coal.

In Xie's study, the mining-induced mechanical behavior of coal masses is confirmed to be quite different from the results of the CTC tests (Xie et al. 2011). The volumetric strain is typically positive throughout the CTC testing process, indicating that the coal specimen is under compression during the entire loading procedure without volumetric expansion relative to its initial state. In contrast, the volumetric strain of the coal specimen in this test is typically negative, which means that the volume of the coal mass continuously increases throughout the mining process. Based on the typical definitions of volumetric strain and porosity, these two parameters have the following relationship:

$$\phi = \frac{\phi_0 - \varepsilon_v}{1 - \varepsilon_v} \tag{7}$$

From Eq. 7, the porosity variation of coal $\Delta\phi$ is obtained as

$$\Delta\phi = \frac{-\varepsilon_v(1 - \phi_0)}{1 - \varepsilon_v} \tag{8}$$

The initial porosity and volumetric strain of a coal specimen are less than one; therefore, $\Delta\phi$ is positive when the volumetric strain is negative. According to Fig. 7 and the relevant analyses in Sect. 4.2, the volumetric strain of the coal mass continuously decreases from the initial zero setting state, which indicates that the porosity of coal increases during the simulation experiments of a mining-induced stress environment. The permeability and porosity of coal have the following general power law relationship (Zhang et al. 2015b),

$$\frac{k}{k_0} = \left(\frac{\phi}{\phi_0}\right)^{\alpha} = \left(1 + \frac{\Delta\phi}{\phi_0}\right)^{\alpha} \tag{9}$$

where α is the porosity sensitivity exponent and is typically greater than two for coal. From Eq. 9, the increment of the coal permeability Δk can be calculated as

$$\Delta k = \left[\left(1 + \frac{\Delta\phi}{\phi_0}\right)^{\alpha} - 1\right] \times k_0 \tag{10}$$

Substituting Eq. 8 into Eq. 10 yields

$$\Delta k = \left[(1 - \frac{\varepsilon_v}{\phi_0})^{\alpha}/(1 - \varepsilon_v)^{\alpha} - 1\right] \times k_0 \tag{11}$$

According to Eq. 11, the coal permeability increases with the volumetric expansion of coal. The simulation of the mining-induced stress evolution process in laboratory testing induces significant volumetric expansion of the coal mass, which makes the coal permeability continuously increase during the loading process without a decreasing section, as in CTC tests. Additionally, the simulation of the pre-mining unloading-expansion process of PCM induces a residual volumetric strain in the coal mass, resulting in an initial MPCR of 200 %. This indicates that the technique of mining the protective coal seam can increase the permeability of protected coal seams and significantly reduce the risk of coal and gas outbursts.

5.2 Field Test Observations

The longwall mining method is widely used in many countries, and the permeability of coal seams, particularly the problem of the MPCR distribution in coal seams, is the subject of continuous research. Estimations of the permeability distribution of coal seams are often conducted in model experiments or numerical simulations. In situ observation is difficult, but the testing results are important and of great reference value for verifying test results.

Adhikary and Guo have investigated the strata permeability induced by longwall mining, in which systematic subsurface and underground hydrogeological monitoring and measurements were conducted, e.g., underground packer tests and piezometer, extensometer, and water inflow monitoring during mining (Adhikary and Guo 2014). Their permeability testing results (Fig. 10) obtained in a solid coal barrier exhibit an evolutionary trend similar to that in Fig. 9, in which a distance of 11.2–11.5 m from the roadway rib yielded the highest average permeability of 89 mD and an average in situ permeability of approximately 1.7 mD (initial permeability) at a distance of 26.2–26.5 m from the roadway rib. The highest MPCR of a coal seam in their study is approximately 5100 %. Their numerical model results (Adhikary and Guo 2015) also match the remaining field permeability measurement data
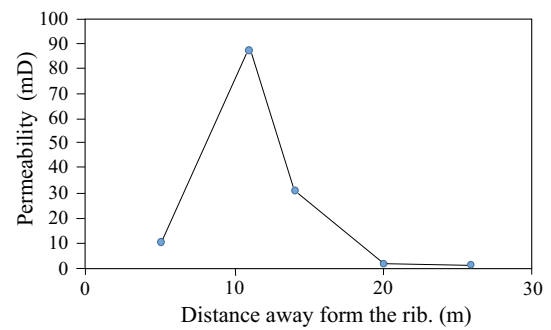

Fig. 10 Permeability estimated using the injection tests versus the distance into the solid coal rib (Adhikary and Guo 2014)
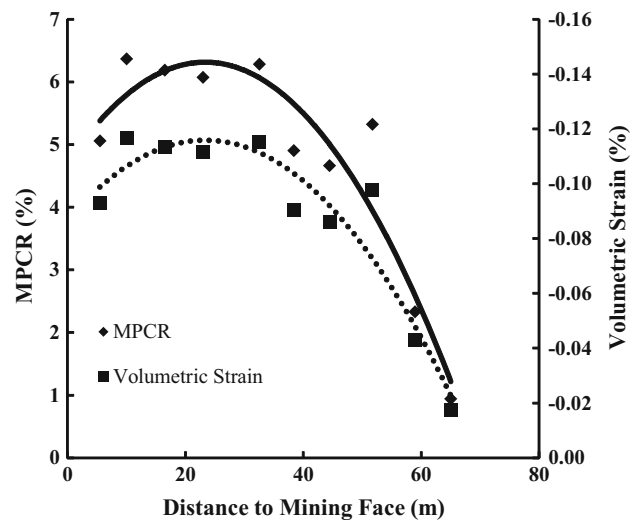

Fig. 11 Evolution of volumetric strain and MPCR of a protective layer with mining face advancement (Xie et al. 2015)

reasonably well. Considering the size effect of laboratory testing, the permeability of a small coal specimen is typically lower than that of an in situ coal mass; thus, the monitoring results are consistent with the testing data in this study. Xie et al. (2015) have conducted field tests in the Pingdingshan Coal Mining Group No. 10 mine and reported a similar MPCR distribution trend in coal seams (see Fig. 11). These field test results are consistent with the testing data from the simulation experiments of the actual mining-induced stress environment in this study, which also confirms the plausibility and practicality of the theoretical expression of MPCR.

6 Conclusions

To comprehensively understand the evolution of coal permeation capacity under different mining layouts, the theoretical expression of MPCR has been derived based on Darcy's law and validated by laboratory experiments and

in situ observations. The MPCR has simple relationships with the gas flow rate and volumetric strain, and it can be measured in situ and used to quantitatively describe the mining-induced permeability change of coal seams under different mining layouts. This is of strong scientific interest for the quantitative evaluation of the CBM extraction arrangement.

Laboratory experiments on the mechanical and permeation properties of coal mass have been conducted under a constant pore pressure difference considering the actual mining-induced stress evolution processes of three typical longwall mining layouts. Also, the pre-mining unloading-expansion process for protected coal seams induced by mining the protective coal seam is also analyzed and simulated in a laboratory. The coal mass has distinguishing mechanical behaviors and permeation properties under the different mining layouts. The coal mass has the lowest peak stress and highest peak MPCR under PCM, reaching approximately 4000 %, whereas the coal mass under NM has the highest peak stress and lowest peak MPCR. The testing results for the coal mass under TCM fall in between these values. Accordingly, the testing results indicate that the PCM is not only a fundamental mining layout but also the most efficient precaution measure. It can strongly increase the MPCR of protected coal seams and reduce the risk of coal and gas outbursts.

The MPCR and volumetric strain variation process of coal mass are obtained according to the theoretical analyses and laboratory testing results. There is a good correspondence between the volumetric strain and MPCR of the coal mass, which show a similar evolution in this study. The evolution process can be divided into three sections, i.e., stable increasing section, accelerated increasing section, and decreasing section. However, the evolution processes are slightly different for the different mining layouts. The rates of increase in the MPCR of the coal mass in the stable increasing section and accelerated increasing section successively increase in the order of NM, TCM, and PCM.

The laboratory testing results can be applied to the field coal seams for mining-induced stress and MPCR distribution analyses based on simplifying assumptions. The MPCR of a coal seam increases with decreasing distance from the mining face before reaching the peak mining-induced stress, and it decreases with the distance from the mining face as a result of the severe coal mass damage and decline in effective flow paths under NM and TCM. The MPCR of the protected coal seam increases with decreasing distance from the mining face due to the effect of the pre-mining unloading-expansion. The distance between the inflection point of the MPCR evolution process and the mining face L_{rise} decreases in the order of NM, TCM, and PCM. L_{rise} decreases in the order of NM, TCM, and PCM, and the MPCR of a coal seam in the range of L_{rise} is larger than 30 %. The ascertainment of L_{rise} is valuable for determining the time and emphasis range of the CBM extraction.

According to the results and analyses in this study, the mining-induced stress evolution processes of different mining layouts influence the mechanical and permeation properties of coal. These results are quite different from those of the CTC tests. Relevant studies should consider the influence of the mining-induced stress evolution process.

References

Adhikary DP, Guo H (2014) Measurement of longwall mining induced strata permeability. Geotech Geol Eng 32(3):617–626

Adhikary DP, Guo H (2015) Modelling of longwall mining-induced strata permeability change. Rock Mech Rock Eng 48(1):345–359

Alehossein H, Poulsen BA (2010) Stress analysis of longwall top coal caving. Int J Rock Mech Min Sci 47(1):30–41

Beamish B, Crosdale PJ (1998) Instantaneous outbursts in underground coal mines: an overview and association with coal type. Int J Coal Geol 35(1):27–55

Cai Y et al (2014) Permeability evolution in fractured coal—combining triaxial confinement with X-ray computed tomography, acoustic emission and ultrasonic techniques. Int J Coal Geol 122:91–104

Cao Y, Mitchell GD, Davis A, Wang D (2000) Deformation metamorphism of bituminous and anthracite coals from China. Int J Coal Geol 43:227–242

Cappa F, Rutqvist J (2011) Modeling of coupled deformation and permeability evolution during fault reactivation induced by deep underground injection of CO_2. Int J Greenhouse Gas Control 5(2):336–346

Chen Z, Pan Z, Liu J, Connell LD, Elsworth D (2011) Effect of the effective stress coefficient and sorption-induced strain on the evolution of coal permeability: experimental observations. Int J Greenhouse Gas Control 5(5):1284–1293

Chen Z, Liu J, Pan Z, Connell LD, Elsworth D (2012) Influence of the effective stress coefficient and sorption-induced strain on the evolution of coal permeability: model development and analysis. Int J Greenhouse Gas Control 8:101–110

Chen H-D, Cheng Y, Zhou H-X, Li W (2013) Damage and permeability development in coal during unloading. Rock Mech Rock Eng 46(6):1377–1390

Chen H, Cheng Y, Ren T, Zhou H, Liu Q (2014) Permeability distribution characteristics of protected coal seams during unloading of the coal body. Int J Rock Mech Min Sci 71:105–116

Cui X, Bustin RM (2005) Volumetric strain associated with methane desorption and its impact on coalbed gas production from deep coal seams. Aapg Bulletin 89(9):1181–1202

Dabbous M, Reznik A, Taber J, Fulton P (1974) The permeability of coal to gas and water. Soc Petrol Eng J 14(06):563–572

Deng J, Yue Z, Tham L, Zhu H (2003) Pillar design by combining finite element methods, neural networks and reliability: a case study of the Feng Huangshan copper mine, China. Int J Rock Mech Min Sci 40(4):585–599

Diederichs M, Kaiser P, Eberhardt E (2004) Damage initiation and propagation in hard rock during tunnelling and the influence of

near-face stress rotation. Int J Rock Mech Min Sci 41(5):785–812

Durucan S, Edwards J (1986) The effects of stress and fracturing on permeability of coal. Mining Sci Technol 3(3):205–216

Flores RM (1998) Coalbed methane: from hazard to resource. Int J Coal Geol 35(1):3–26

Gale JE (1982) The effects of fracture type (induced versus natural) on the stress-fracture closure-fracture permeability relationships. In: The 23rd US Symposium on Rock Mechanics (USRMS). American Rock Mechanics Association, Berkeley

Gilman A, Beckie R (2000) Flow of coal-bed methane to a gallery. Transp Porous Media 41(1):1–16

Gray I (1987) Reservoir engineering in coal seams: part 1-The physical process of gas storage and movement in coal seams. SPE Reser Eng 2(1):28–34

Guo H, Yuan L, Shen B, Qu Q, Xue J (2012) Mining-induced strata stress changes, fractures and gas flow dynamics in multi-seam longwall mining. Int J Rock Mech Min Sci 54(3):129–139

Harpalani S, Chen G (1997) Influence of gas production induced volumetric strain on permeability of coal. Geotech Geol Eng 15(4):303–325

Klinkenberg L (1941) The permeability of porous media to liquids and gases. Drilling and production practice. American Petroleum Institute, New York, pp 200–213

Kong S, Cheng Y, Ren T, Liu H (2014) A sequential approach to control gas for the extraction of multi-gassy coal seams from traditional gas well drainage to mining-induced stress relief. Appl Energy 131(9):67–78

Li Z, Dou L, Cai W, Wang G, Ding Y, Kong Y (2015) Roadway stagger layout for effective control of gob-side rock bursts in the longwall mining of a thick coal seam. Rock Mech Rock Eng. doi:10.1007/s00603-015-0746-6

Liu J, Chen Z, Elsworth D, Miao X, Mao X (2010) Linking gas-sorption induced changes in coal permeability to directional strains through a modulus reduction ratio. Int J Coal Geol 83(1):21–30

Liu Y, Zhou F, Liu L, Liu C, Hu S (2011) An experimental and numerical investigation on the deformation of overlying coal seams above double-seam extraction for controlling coal mine methane emissions. Int J Coal Geol 87(2):139–149

Liu Q, Cheng Y, Zhou H, Guo P, An F, Chen H (2014) A mathematical model of coupled gas flow and coal deformation with gas diffusion and klinkenberg effects. Rock Mech Rock Eng 48(3):1163–1180

Mazumder S, Wolf KH (2008) Differential swelling and permeability change of coal in response to CO_2 injection for ECBM. Int J Coal Geol 74(2):123–138

Meng Z, Li G (2013) Experimental research on the permeability of high-rank coal under a varying stress and its influencing factors. Eng Geol 162(14):108–117

Moore TA (2012) Coalbed methane: a review. Int J Coal Geol 101(6):36–81

Ouyang Z, Li C, Xu W, Li H (2009) Measurements of in situ stress and mining-induced stress in Beiminghe Iron Mine of China. J Cent South Univ Technol 16(1):85–90

Palmer I (2009) Permeability changes in coal: analytical modeling. Int J Coal Geol 77(1):119–126

Pan Z, Connell LD, Camilleri M (2010) Laboratory characterisation of coal reservoir permeability for primary and enhanced coalbed methane recovery. Int J Coal Geol 82(3):252–261

Perera M, Ranjith P, Choi S, Bouazza A, Kodikara J, Airey D (2011) A review of coal properties pertinent to carbon dioxide sequestration in coal seams: with special reference to Victorian brown coals. Environ Earth Sci 64(1):223–235

Perera M, Ranjith P, Choi S, Airey D (2012) Investigation of temperature effect on permeability of naturally fractured black

coal for carbon dioxide movement: an experimental and numerical study. Fuel 94:596–605

Raven K, Gale J (1985) Water flow in a natural rock fracture as a function of stress and sample size. Int J Rock Mech Min Sci Geomech Abst 22(4):251–261

Rezaei M, Hossaini MF, Majdi A (2015) Determination of longwall mining-induced stress using the strain energy method. Rock Mech Rock Eng 2015:1–13. doi:10.1007/s00603-014-0704-8

Ried G, Towler B, Harris H (1992) Simulation and economics of coalbed methane production in the Powder River Basin. In: SPE Rocky Mountain Regional Meeting. Society of Petroleum Engineers, Casper, Wyoming, USA. Paper 24360. doi:10.2118/24360-MS

Robertson EP, Christiansen RL (2007) Modeling laboratory permeability in coal using sorption-induced strain data. SPE Reservoir Eval Eng 10(3):260–269

Shi J, Durucan S (2004) Drawdown induced changes in permeability of coalbeds: a new interpretation of the reservoir response to primary recovery. Transp Porous Media 56(1):1–16

Singh AK, Singh R, Maiti J, Kumar R, Mandal P (2011) Assessment of mining induced stress development over coal pillars during depillaring. Int J Rock Mech Min Sci 48(5):805–818

Siriwardane H, Haljasmaa I, McLendon R, Irdi G, Soong Y, Bromhal G (2009) Influence of carbon dioxide on coal permeability determined by pressure transient methods. Int J Coal Geol 77(1):109–118

Somerton WH, Söylemezoḡlu I, Dudley R (1975) Effect of stress on permeability of coal. Int J Rock Mech Min Sci Geomech Abst 12(5):129–145

Sparks D, McLendon T, Saulsberry J, Lambert S The effects of stress on coalbed reservoir performance, Black Warrior Basin, USA. In: Society of Petroleum Engineers. Annual Technical Conference, Dallas, TX, USA 1995. pp 339–351 doi:10.2118/30734-MS

Suchowerska A, Merifield R, Carter J (2013) Vertical stress changes in multi-seam mining under supercritical longwall panels. Int J Rock Mech Min Sci 61:306–320

Wang L, Cheng Y-P, Li F-R, Wang H-F, H-b Liu (2008) Fracture evolution and pressure relief gas drainage from distant protected coal seams under an extremely thick key stratum. J China Univ Min Technol 18(2):182–186

Wang G, Wei X, Wang K, Massarotto P, Rudolph V (2010) Sorption-induced swelling/shrinkage and permeability of coal under stressed adsorption/desorption conditions. Int J Coal Geol 83(1):46–54

Wang S, Elsworth D, Liu J (2011) Permeability evolution in fractured coal: the roles of fracture geometry and water-content. Int J Coal Geol 87(1):13–25

Wang C, Zhang N, Han Y, Xiong Z, Qian D (2013a) Experiment research on overburden mining-induced fracture evolution and its fractal characteristics in ascending mining. Arab J Geosci 8(1):13–21

Wang H, Jiang Y, Zhao Y, Zhu J, Liu S (2013b) Numerical investigation of the dynamic mechanical state of a coal pillar during longwall mining panel extraction. Rock Mech Rock Eng 46(5):1211–1221

Wang S, Elsworth D, Liu J (2013c) Permeability evolution during progressive deformation of intact coal and implications for instability in underground coal seams. Int J Rock Mech Min Sci 58:34–45

Whittaker B (1974) An appraisal of strata control practice. Min Eng 134:9–24

Xie G, Chang J, Yang K (2009) Investigations into stress shell characteristics of surrounding rock in fully mechanized top-coal caving face. Int J Rock Mech Min Sci 46(1):172–181

Xie H, Zhou H, Liu J, Xue D (2011) Mining-induced mechanical behavior in coal seams under different mining layouts. J China Coal Soc 36(7):1067–1074 **(in Chinese)**

Xie H, Zhao X, Liu J, Zhang R, Xue D (2012) Influence of different mining layouts on the mechanical properties of coal. Int J Min Sci Technol 22(6):749–755

Xie H, Gao F, Zhou H-W, Cheng H-M, Zhou F-B (2013) On theoretical and modeling approach to mining-enhanced permeability for simultaneous exploitation of coal and gas. J China Coal Soc 38(7):1101–1108 **(in Chinese)**

Xie H, Xie J, Gao M, Zhang R, Zhou H, Gao F, Zhang Z (2015) Theoretical and experimental validation of mining-enhanced permeability for simultaneous exploitation of coal and gas. Environ Earth Sci 73(10):5951–5962

Yang W, Lin B, Qu Y, Li Z, Zhai C, Jia L, W-q Zhao (2011) Stress evolution with time and space during mining of a coal seam. Int J Rock Mech Min Sci 48(7):1145–1152

Yang W, B-q Lin, Yan Q, Zhai C (2014) Stress redistribution of longwall mining stope and gas control of multi-layer coal seams. Int J Rock Mech Min Sci 72:8–15

Yasitli N, Unver B (2005) 3D numerical modeling of longwall mining with top-coal caving. Int J Rock Mech Min Sci 42(2):219–235

Zhang H, Liu J, Elsworth D (2008) How sorption-induced matrix deformation affects gas flow in coal seams: a new FE model. Int J Rock Mech Min Sci 45(8):1226–1236

Zhang M, Shimada H, Sasaoka T, Matsui K, Dou L (2014a) Evolution and effect of the stress concentration and rock failure in the deep multi-seam coal mining. Environ Earth Sci 72(3):629–643

Zhang Z, Zhang R, Liu J, Liu X, Li J (2014b) Permeability evolution of unloaded coal samples at different loading rates. Thermal Sci 18(5):1497–1504

Zhang R, Ai T, Zhou HW, Ju Y, Zhang ZT (2015a) Fractal and volume characteristics of 3D mining-induced fractures under typical mining layouts. Environ Earth Sci 73(10):6069–6080

Zhang Z, Zhang R, Xie H, Gao M (2015b) The relationships among stress, effective porosity and permeability of coal considering the distribution of natural fractures: theoretical and experimental analyses. Environ Earth Sci 73(10):5997–6007

Zhou C, Yao Y, Guo L, Yin X, Fan X, Shang Y (2007) Numerical simulation of independent advance of ore breaking in the non-pillar sublevel caving method. J China Univ Min Technol 17(2):295–300

Zhu W, Liu J, Sheng J, Elsworth D (2007) Analysis of coupled gas flow and deformation process with desorption and Klinkenberg effects in coal seams. Int J Rock Mech Min Sci 44(7):971–980

Zhu WC, Wei CH, Liu J, Xu T, Elsworth D (2013) Impact of gas adsorption induced coal matrix damage on the evolution of coal permeability. Rock Mech Rock Eng 46(6):1353–1366